High-Spin Molecules: $(NBu^n_4)[Mn_8O_6Cl_6(O_2CPh)_7(H_2O)_2]$ (S = 11) and $[Mn_9Na_2O_7(O_2CPh)_{15}(MeCN)_2]$ (S = 4)

Hui-Lien Tsai,[1] Sheyi Wang,[2] Kirsten Folting,[2] William E. Streib,[2] David N. Hendrickson,*[,1] and George Christou*[,2]

Contribution from the Department of Chemistry and Molecular Structure Center, Indiana University, Bloomington, Indiana 47405-4001, and Department of Chemistry—0358, University of California at San Diego, La Jolla, California 92093-0358

Received August 23, 1994[⊗]

Abstract: The syntheses and electrochemical and magnetochemical properties of $(NBu^n_4)[Mn_8O_6Cl_6(O_2CPh)_7(H_2O)_2]\cdot xCH_2Cl_2$ ($2\cdot xCH_2Cl_2$) and $[Mn_9Na_2O_7(O_2CPh)_{15}(MeCN)_2]\cdot 3MeCN$ ($3\cdot 3MeCN$) are reported. Both complexes were prepared from reactions involving $(NBu^n_4)[Mn_4O_2(H_2O)(O_2CPh)_9]$ (**1**). Complex **2** was obtained in 45–60% yield on treatment of complex **1** with 4 equiv of Me_3SiCl in CH_2Cl_2. Complex $2\cdot 3/2CH_2Cl_2\cdot 2H_2O$ crystallizes in triclinic space group $P\bar{1}$ with the following cell parameters at −169 °C: a = 16.104(4) Å, b = 21.501(6) Å, c = 14.843(4) Å, α = 94.24(1)°, β = 105.96(1)°, γ = 89.07(1)°, V = 4927.79 Å^3, and Z = 2. The structure was refined by employing 10 108 unique reflections with $F > 3.0\sigma(F)$ to give R = 0.0912 and R_w = 0.0944. Complex **2** contains a $[Mn_8O_6Cl_4]^{8+}$ core ($8Mn^{III}$) that may be conveniently described as resulting from the fusion of two $[Mn_4O_2]$ butterfly units by sharing one "body" or "hinge" Mn. An eighth Mn^{III} ion is connected to the resultant $[Mn_7O_4]$ unit by two additional bridging O^{2-} ions. Complex **3** was obtained in 31% yield from the treatment of complex **1** with 1 equiv of benzoyl peroxide in MeCN, followed by addition of $NaClO_4$. Complex $3\cdot 3MeCN$ crystallizes in triclinic space group $P\bar{1}$ with the following cell parameters at −170 °C: a = 15.116(2) Å b = 27.903(4) Å, c = 15.007(2) Å, α = 102.40(1)°, β = 112.36(1)°, γ = 84.17(1)°, V = 5715.26 Å^3, and Z = 2. The structure was refined by employing 12 020 unique reflections with $F > 3\sigma(F)$ to give R = 0.0514 and R_w = 0.0525. Complex **3** possesses a mixed-metal undecanuclear $[Mn_9Na_2O_7]^{15+}$ core ($9Mn^{III}$); the Mn_9O_7 subcore again comprises a $[Mn_7O_4]$ unit constructed from the fusion, in the same manner as for complex **2**, of two $[Mn_4O_2]$ butterfly units. There are now two additional Mn^{III} ions connected to the $[Mn_7O_4]$ unit, by three additional bridging O^{2-} ions. The Na^+ ions are bound to bridging O^{2-} ions of the $[Mn_9O_7]$ core, supporting a heterometallic-aggregate description rather than an ion-pairing description. Complex **2** displays reversible redox couples when examined by cyclic voltammetry in CH_2Cl_2; an oxidation and a reduction are observed at 0.91 and 0.12 V, respectively, *vs* ferrocene. Complex **3** displays no reversible processes. Variable-temperature and variable-field dc magnetic susceptibility data were collected for polycrystalline samples of complexes **2** and **3**. In a 10.0 kG field, $\chi_M T$ for complex **2** increases with decreasing temperature from 23.7 cm^3 K mol^{-1} (μ_{eff} = 13.8 μ_B) at 300.0 K to a maximum of 53.2 cm^3 K mol^{-1} (μ_{eff} = 20.6 μ_B) at 15.0 K, whereupon there is a decrease to 39.3 cm^3 K mol^{-1} (μ_{eff} = 17.7 μ_B) at 5.01 K. The shape of this $\chi_M T$ *vs* temperature curve reflects the population of a S = 11 ground state at low temperature. Least-squares fitting of reduced magnetization *vs* H/T data for complex **2** in the 2.0–30.0 K and 5.00–50.0 kG field range confirms that complex **2** has a S = 11 ground state with g = 1.92 and axial zero-field splitting of D = −0.04 cm^{-1}. The ac susceptibility data measured in zero external field for complex **2** in the 2.0–30.0 K range also indicate a S = 11 ground state. No out-of-phase ac magnetic susceptibility signal was observed for complex **2** in the 2.0–30.0 K range in spite of its large-spin ground state. The absence of an out-of-phase ac signal is attributable to a very small zero-field splitting in the S = 11 ground state, and the small D-value results from a near cancellation of single-ion zero-field interactions at the eight Mn^{III} ions in complex **2**. Complex **3** exhibits dc and ac magnetic susceptibility data consistent with a S = 4 ground state. In a 10.0 kG field μ_{eff} decreases gradually from 12.23 μ_B at 320 K to 6.94 μ_B at 5.01 K. Even though there are some similarities in molecular structure between complexes **2** and **3**, differences in the nature of spin frustration result in a S = 11 ground state for complex **2** and a S = 4 ground state for complex **3**.

Introduction

The preparation of molecules with large numbers of unpaired electrons represents an area of considerable interest because it is widely recognized that such molecules are potential building blocks for molecular-based magnetic materials.[3] A number of strategies are currently available to access the latter: (i) salt formation between metallocene cation (D^+) and organic anions (A^-), each with an unpaired elctron (S = $^1/_2$), arranged in alternating stacks;[4] (ii) formation of ferrimagnetic chains consisting of bridged heterometallic (Cu^{II}–L–Mn^{II}) (L = a bridging organic group) building blocks;[5a,b] (iii) formation of covalently-linked heterospin chains as in strategy ii, but with

⊗ Abstract published in *Advance ACS Abstracts,* February 1, 1995.

(1) University of California at San Diego.

(2) Indiana University.

(3) (a) *Magnetic Molecular Materials*; Gatteschi, D., Kahn, O., Miller, J. S., Palacio, F., Eds.; NATO ASI Series E, 198; Kluwer Academic Publishers: Dordrecht, The Netherlands, 1991. (b) Kahn, O.; Pei, Y.; Journaux, Y. Molecular Inorganic Magnetic Materials. In *Inorganic Materials*; Bruce, D. W., O'Hare, D., Eds.; Wiley & Sons Ltd.: New York, 1992; pp 59–114.

(4) (a) Miller, J. S.; Epstein, A. J.; Reiff, W. M. *Chem. Rev.* **1988**, *88*, 201. (b) Miller, J. S.; Epstein, A. J.; Reiff, W. M. *Acc. Chem. Res.* **1988**, *21*, 114. (c) Miller, J. S.; Epstein, A. J. *Angew. Chem., Int. Ed. Engl.* **1994**, *33*, 385–415.

(5) (a) Kahn, O. *Struct. Bonding (Berlin)* **1987**, *68*, 89. (b) Kahn, O.; Pei, Y.; Nakatani, K.; Journaux, Y. *Mol. Cryst. Liq. Cryst.* **1989**, *176*, 481. (c) Stumpf, H. O.; Ouahab, L.; Pei, Y.; Grandjean, D.; Kahn, O. *Science* **1993**, *261*, 447. (d) Stumpf, H. O.; Ouahab, L.; Pei, Y.; Bergerat, P.; Kahn, O. *J. Am. Chem. Soc.* **1994**, *116*, 3866.

0002-7863/95/1517-2503$09.00/0

one of the alternating species possessing unpaired electrons on an organic group[6] (thus, chains consisting of alternating metal ions and nitroxide ($S = {}^1/_2$) groups have been prepared and found to exhibit ferromagnetism); (iv) formation of covalently-linked heterospin chains as above, but involving *three* spin centers, two of which are metals (Mn^{II}, Cu^{II}) and the third of which is an organic radical group;[5c,d] and (v) construction of three-dimensional lattices with oxalate[7a-c] or cyanide[7d,e] bridges.

It is clear that the types of studies described above establish the feasibility of preparing molecular-based ferromagnets; the continuing challenge is to extend these and related approaches to other molecules possessing unpaired electrons. In particular, it is important to access new molecular species with large spin values in the ground state and to develop the manipulative methodology to link these species in an appropriate manner so as to allow long-range ferro- and/or ferrimagnetic ordering in three dimensions. The search for molecules with large numbers of unpaired electrons is being pursued in both the organic[8-10] and inorganic areas. In the inorganic area, an $[Mn^{II}_6(\text{nitroxide})_6]$ complex has been prepared that has a $S = 12$ ground state.[11] Very recently Goldberg *et al.*[12] reported the preparation and characterization of $(Me_4N)_4[Mn_{10}(\text{biphen})_4O_4Cl_{12}]$, where biphen is 2,2′-biphenoxide. This $Mn^{II}_6Mn^{III}_4$ complex was shown to have a $S = 14$ ground state, which is the record for the highest spin ground state of any molecular species.

The complex $[Mn_{12}O_{12}(O_2CMe)_{16}(H_2O)_4]$ (**5**) has a $S = 10$ ground state in zero field, and $[Mn_{12}O_{12}(O_2CPh)_{16}(H_2O)_4]$ (**4**) has a $S = 10$ or $S = 9$ ground state in a ≥20 kG field, depending on whether the complex has no or some interstitial molecules in the crystal lattice.[13] Most interestingly, these Mn_{12} complexes are the only molecular species known to exhibit a nonzero, out-of-phase (imaginary) component in their ac susceptibility response in zero applied field.[13-15] In addition, measurements performed at various frequencies show that the temperature at which the maximum in the imaginary component occurs is frequency-dependent. Paramagnets display an out-of-phase ac response only in the presence of an external magnetic field. In contrast, materials with a spontaneous magnetization below some critical temperature (T_c) can show an out-of-phase response in zero applied field, but in this case, the temperatures at which the maxima occur are not frequency-dependent. Frequency-dependent maxima have been observed to date for superparamagnets[16] and spin glasses.[17] Thus, these Mn_{12} complexes are exhibiting behavior not normally associated with small molecular species.

It is obvious from the above discussion that the study of additional examples of molecular Mn_x aggregates with large ground state spin values would be highly desirable and important to achieving an understanding of the origin of these unusual ac susceptibility relaxation effects. This requires synthetic access to pure materials in sufficient amounts and with large values of S.[18] In the present work, we report two new high-nuclearity molecular Mn_x species with $x = 8$ or 9 and describe their structural and magnetochemical characterization. Portions of this work have been briefly communicated.[19]

Experimental Section

Compound Preparations. All materials, except those indicated below, were used as received. $(NBu^n_4)[Mn_4O_2(H_2O)(O_2CPh)_9]$[19] (**1**) was prepared as described elsewhere. MeCN and CH_2Cl_2 were distilled from CaH_2; Et_2O was distilled from Na/benzophenone.

$(NBu^n_4)[Mn_8O_6Cl_6(O_2CPh)_7(H_2O)_2]$ (2). To a stirred red-brown solution of complex **1** (0.48 g, 0.30 mmol) in CH_2Cl_2 (20 mL) was added Me_3SiCl (0.15 mL, 1.2 mmol). No significant color change occurred. The flask was kept at room temperature for several hours, and then Et_2O (40 mL) was added to yield a dark red precipitate. This was collected by filtration, washed well with Et_2O, and dried in air. The solid was recrystallized from CH_2Cl_2/Et_2O as dark red crystals of $\mathbf{2}\cdot{}^3/_2CH_2Cl_2\cdot 2H_2O$. Typical yields are in the 47−58% range. A sample for crystallography was kept in contact with the mother liquor to prevent interstitial solvent loss. Collection of the crystals by filtration, washing with Et_2O, and drying *in vacuo* leads to the unsolvated form. Anal. Calcd (found) for $C_{65}H_{75}NO_{22}Cl_6Mn_8$: C, 41.65 (41.3); H, 4.03 (4.0); N, 0.75 (0.7); Cl, 11.35 (10.8). Electronic spectrum in CH_2Cl_2: λ_{max}, nm (ϵ_M, L mol^{-1} cm^{-1}); 442 (4200), 488 (3510). Selected IR data (Nujol mull): 3400 (m, br), 1599 (m), 1539 (m, sh), 1516 (s), 1493 (m), 721 (s), 683 (m), 664 (s), 628 (m), 598 (s).

$[Mn_9Na_2O_7(O_2CPh)_{15}(MeCN)_2]$ (3). To a stirred red-brown solution of complex **1** (0.80 g, 0.50 mmol) in MeCN (40 mL) was added solid dibenzoyl peroxide (0.12 g, 0.50 mmol). After the latter had completely dissolved, $NaClO_4$ (0.13 g, 1.0 mmol) was added, and the mixture was stirred overnight. The resulting homogeneous solution was allowed to stand undisturbed for several days. Large black crystals of **3**·MeCN were collected by filtration, washed with MeCN, and dried *in vacuo*. The crystallographic sample was maintained in contact with the mother liquor; dried solid loses interstitial MeCN and appears to be hygroscopic, analyzing for $\mathbf{3}\cdot{}^3/_2H_2O$. Anal. Calcd (found) for $C_{109}H_{84}N_2O_{38.5}N_2Mn_9$: C, 50.78 (50.8); H, 3.28 (3.4); N, 1.09 (0.85); Mn, 19.18 (18.8). Electronic spectrum in CH_2Cl_2: λ_{max}, nm (ϵ_M, L mol^{-1} cm^{-1}), 486 (3100), 542 (sh, ~2600), ~616 (sh, 1500). Selected IR data (Nujol): 3360 (w, br), 1597 (s), 1555 (s), 1531 (s, sh), 1512 (s, sh), 1493 (s), 719 (s), 685 (s), 648 (s).

X-ray Crystallography and Structure Solution. Data were collected on a Picker four-circle diffractometer at −169 and −170 °C for complexes **2** and **3**, respectively; details of the diffractometry, low-temperature facilities, and computational procedures employed by the Molecular Structure Center are available elsewhere.[20] Crystals of the two complexes, maintained in contact with mother liquor to prevent solvent loss, were affixed to glass fibers with silicone grease and quickly transferred to a goniometer, where they were cooled for characterization and data collection. For both complexes, a systematic search of reciprocal space revealed no Laue symmetry or systematic extinctions. Initial choices of space group $P\bar{1}$ were proven correct by subsequent successful solution of the structure. The structures were solved using a combination of direct methods (MULTAN) and Fourier techniques and were refined by full-matrix least-squares. No absorption corrections were performed.

For complex **2**, the positions of the Mn atoms were obtained from an initial *E*-map. The remaining atoms were obtained by iterations of

(6) Caneschi, A.; Gatteschi, D.; Sessoli, R.; Rey, P. *Acc. Chem. Res.* **1989**, *22*, 392.
(7) (a) Tamaki, H.; Zhong, Z. J.; Matsumoto, N.; Kida, S.; Koikawa, M.; Achiwa, N.; Hashimoto, Y.; Okawa, H. *J. Am. Chem. Soc.* **1992**, *114*, 6974. (b) Mathonière, C.; Carling, S. G.; Yusheng, D.; Day, P. *J. Chem. Soc., Chem. Commun.* **1994**, 1551. (c) Decurtins, S.; Schmalle, H. W.; Schneuwly, P.; Ensling, J.; Gütlich, P. *J. Am. Chem. Soc.* **1994**, *116*, 9521. (d) Gadet, V.; Mallah, T.; Castro, I.; Verdaguer, M. *J. Am. Chem. Soc.* **1992**, *114*, 9213. (e) Entley, W. R.; Girolami, G. S. *Inorg. Chem.* **1994**, *33*, 5165.
(8) (a) Iwamura, H. *Pure Appl. Chem.* **1987**, *59*, 1595. (b) Iwamura, H. *Pure Appl. Chem.* **1986**, *58*, 187. (c) Itoh, K.; Takui, T.; Teki, Y.; Kinoshita, J. *J. Mol. Elect.* **1988**, *4*, 181.
(9) Nakamura, N.; Inoue, K.; Iwamura, H.; Fujioka, T.; Sawaki, Y. *J. Am. Chem. Soc.* **1992**, *114*, 1484.
(10) Dougherty, D. A. *Pure Appl. Chem.* **1990**, *62*, 519.
(11) Caneschi, A.; Gatteschi, D.; Laugier, J.; Rey, P.; Sessoli, R.; Zanchini, C. *J. Am. Chem. Soc.* **1988**, *110*, 2795.
(12) Goldberg, D. P.; Caneschi, A.; Lippard, S. J. *J. Am. Chem. Soc.* **1993**, *115*, 9299.
(13) Sessoli, R.; Tsai, H.-L.; Schake, A. R.; Wang, S.; Vincent, J. B.; Folting, K.; Gatteschi, D.; Christou, G.; Hendrickson, D. N. *J. Am. Chem. Soc.* **1993**, *115*, 1804.
(14) Caneschi, A.; Gatteschi, D.; Sessoli, R.; Barra, A. L.; Brunel, L. C.; Guillot, M. *J. Am. Chem. Soc.* **1991**, *113*, 5873.
(15) Caneschi, A.; Gatteschi, D.; Sessoli, R.; Novak, M. A. *Nature* **1993**, *365*, 141.
(16) Richardson, J. T.; Milligan, W. D. *Phys. Rev. B* **1956**, *102*, 1289.
(17) Nagata, S.; Keesom, P. H.; Harrison, H. N. *Phys. Rev. B* **1979**, *19*, 1363.
(18) Wemple, M. W.; Tsai, H.-L.; Streib, W. E.; Hendrickson, D. N.; Christou, G. *J. Chem. Soc., Chem. Commun.* **1994**, 1031.
(19) Wang, S.; Huffman, J. C.; Folting, K.; Streib, W. E.; Lobkovsky, E. B.; Christou, G. *Angew. Chem., Int. Ed. Engl.* **1991**, *30*, 1672.
(20) Chisholm, M. F.; Folting, K.; Huffman, J. C.; Kirkpatrick, C. C. *Inorg. Chem.* **1984**, *23*, 1021.

Table 1. Crystallographic Data for Complexes **2**·3/2CH_2Cl_2·2H_2O and **3**·3MeCN

	2	**3**
formula	$C_{66.5}H_{82}NO_{24}Cl_9Mn_8$[a]	$C_{115}H_{90}N_5O_{37}Na_2Mn_9$[a]
formula wt, g/mol	2037.96[a]	2674.46[a]
space group	$P\bar{1}$	$P\bar{1}$
a, Å	16.104(4)	15.116(2)
b, Å	21.501(6)	27.903(4)
c, Å	14.843(4)	15.007(2)
α, deg	94.24(1)	102.40(1)
β, deg	105.96(1)	112.36(1)
γ, deg	89.07(1)	84.17(1)
V, Å^3	4927.79	5715.26
Z	2	2
T, °C	−169	−170
radiation[b]	0.710 69	0.710 69
ϱ_{calc}, g/cm^3	1.375	1.554
μ, cm^{-1}	13.395	10.115
octants	$+h,\pm k,\pm l$	$+h,\pm k,\pm l$
total data	26 156	19 595
unique data	12 920	14 992
R_{merge}	0.045	0.035
obsd data ($F > 3\sigma(F)$)	10 108	12 020
R (R_w)[c,d]	0.0912 (0.0944)	0.0514 (0.0525)

[a] Including solvate molecules. [b] Graphite monochromator. [c] $R = \sum||F_o| - |F_c||/\sum|F_o|$. [d] $R_w = [\sum w(|F_o| - |F_c|)^2/\sum w|F_o|^2]^{1/2}$ where $w = 1/\sigma^2(|F_o|)$.

least-squares refinement and difference Fourier map calculations. One phenyl ring (C(78)−C(83)) in the anion and one butyl group (C(95)−C(98)) in the cation are disordered. The phenyl ring was modeled as four carbon atoms plus four half-weight carbon atoms, and the butyl group was modeled as two carbon atoms plus four half-weight carbon atoms. The asymmetric unit also contains solvent. Three CH_2Cl_2 units were clearly observed although only at approximately half-occupancy. Two additional peaks were observed in well-isolated space; these were included as half-weight oxygens (*i.e.*, water) although they may be additional disordered solvent at even lower occupancy. Hydrogen atoms were included in fixed, calculated positions on the ordered carbon atoms. In the final cycles of refinement, the ordered atoms (98) were refined with anisotropic thermal parameters, and the disordered atoms (17) were refined with isotropic thermal parameters. The final difference Fourier map was essentially featureless, the largest peak being 2.0 e/Å^3 in the vicinity of a solvent molecule. Final R (R_w) values are listed in Table 1.

For complex **3**, the nine Mn atoms were located in the initial E-map and the remaining nonhydrogen atoms were located in subsequent difference Fourier maps. Three disordered interstitial MeCN molecules were also located in the asymmetric unit. Following initial least-squares refinement, many of the hydrogen atoms were located in a difference Fourier map; all benzoate hydrogen atoms were introduced in fixed, idealized positions. Owing to the large number of parameters, the full-matrix least-squares refinement was carried out in a cyclical manner. Atoms Mn(1) through N(159) were refined using anisotropic thermal parameters, while the lattice solvent atoms were refined using isotropic thermal parameters. The final difference Fourier map was essentially featureless, the largest peak being 1.54 e/Å^3 in the vicinity of C(160), a carbon atom in one of the disordered solvent molecules. The final difference Fourier contained six peaks that could be identified as hydrogen atoms on C(154) and C(157) of the well-behaved, bound CH_3CN molecules. However, since the least-squares program has an upper limit of 250 atoms, hydrogen atoms on these solvent molecules were not introduced. Final R (R_w) values are included in Table 1.

Physical Measurements. The dc magnetic susceptibility measurements were carried out on a Quantum Design MPMS5 SQUID susceptometer equipped with a 55 kG magnet and operated in the range 1.8−400 K. The ac magnetic susceptibility measurements were carried out on a Quantum Design MPMS2 SQUID ac susceptometer. The ac frequency range is 5.0×10^{-4} Hz to 1.5 kHz, and the ac field strength can be varied from 10^{-4} to 5.8 G.

Pascal's constants[21] were used to estimate the diamagnetic corrections for each complex, which were subtracted from the experimental susceptibilities to give the molar paramagnetic susceptibilities. The computer program GENSPIN[22] was used to analyze variable-field magnetization data. The spin of the ground state is set at some value, and then the spin Hamiltonian matrix is diagonalized at each magnetic field to least-squares fit the experimental data.

Electrochemical studies were performed by using an IBM Model EC 225 voltammetric analyzer, a PAR Model 175 universal programmer, and a standard three-electrode assembly (glassy-carbon working, Pt-wire auxiliary, SCE reference) with 0.1 M $NBu^n_4PF_6$ as the supporting electrolyte. No ohmic compensation was employed. Quoted potential values are versus the ferrocene/ferrocenium couple measured under the same conditions. The scan rate was set at 100 mV/s for cyclic voltammetry and 5 mV/s for differential pulse voltammetry. The solvent used was distilled CH_2Cl_2, and the concentration of the complexes was approximately 1 mM.

Table 2. Selected Interatomic Distances (Å) for $(NBu^n_4)[Mn_8O_6Cl_6(O_2CPh)_7(H_2O)_2]$ (**2**)

Mn(1)−Mn(2)	2.828(3)	Mn(3)−O(48)	1.945(8)
Mn(1)−Mn(4)	3.145(2)	Mn(3)−O(57)	1.954(7)
Mn(1)−Mn(7)	3.137(3)	Mn(4)−Cl(15)	2.787(3)
Mn(2)−Mn(3)	2.791(3)	Mn(4)−Cl(17)	2.461(4)
Mn(2)−Mn(4)	3.191(2)	Mn(4)−O(9)	1.881(8)
Mn(2)−Mn(5)	3.218(2)	Mn(4)−O(13)	1.878(7)
Mn(2)−Mn(6)	3.197(3)	Mn(4)−O(23)	1.926(8)
Mn(2)−Mn(7)	3.180(3)	Mn(4)−O(66)	1.936(8)
Mn(2)−Mn(8)	3.625(2)	Mn(5)−Cl(16)	2.703(4)
Mn(3)−Mn(5)	3.141(2)	Mn(5)−Cl(17)	2.571(3)
Mn(3)−Mn(6)	3.131(3)	Mn(5)−Cl(19)	2.263(4)
Mn(4)−Mn(5)	3.171(3)	Mn(5)−O(11)	1.867(8)
Mn(4)−Mn(8)	3.150(3)	Mn(5)−O(13)	1.929(8)
Mn(5)−Mn(8)	3.493(3)	Mn(5)−O(50)	1.955(8)
Mn(6)−Mn(7)	3.176(3)	Mn(6)−Cl(16)	2.685(4)
Mn(6)−Mn(8)	3.508(3)	Mn(6)−Cl(18)	2.616(4)
Mn(7)−Mn(8)	3.158(2)	Mn(6)−Cl(20)	2.246(4)
Mn(1)−Cl(15)	2.692(4)	Mn(6)−O(12)	1.883(7)
Mn(1)−O(9)	1.887(8)	Mn(6)−O(14)	1.932(7)
Mn(1)−O(10)	1.872(7)	Mn(6)−O(59)	1.954(8)
Mn(1)−O(21)	1.943(7)	Mn(7)−Cl(15)	2.776(3)
Mn(1)−O(30)	1.953(8)	Mn(7)−Cl(18)	2.466(3)
Mn(1)−O(84)	2.191(9)	Mn(7)−O(10)	1.878(7)
Mn(2)−O(9)	1.900(7)	Mn(7)−O(14)	1.892(8)
Mn(2)−O(10)	1.928(8)	Mn(7)−O(32)	1.944(9)
Mn(2)−O(11)	1.912(8)	Mn(7)−O(75)	1.955(8)
Mn(2)−O(12)	1.901(7)	Mn(8)−Cl(15)	2.709(4)
Mn(2)−O(39)	2.151(8)	Mn(8)−O(13)	1.885(7)
Mn(3)−Cl(16)	2.602(4)	Mn(8)−O(14)	1.891(7)
Mn(3)−O(11)	1.881(7)	Mn(8)−O(68)	1.956(7)
Mn(3)−O(12)	1.888(8)	Mn(8)−O(77)	1.957(7)
Mn(3)−O(41)	2.122(8)	Mn(8)−O(85)	2.184(9)

Results

Two procedures have been developed that lead to conversion of $(NBu^n_4)[Mn_4O_2(H_2O)(O_2CPh)_9]$ (**1**) into higher nuclearity Mn^{III} products. Treatment of complex **1** with 4 equiv of Me_3SiCl in CH_2Cl_2 leads to subsequent isolation of $(NBu^n_4)[Mn_8O_6Cl_6(O_2CPh)_7(H_2O)_2]$ (**2**) in good yields (47−58%). The single-crystal X-ray structure of **2**·3/2CH_2Cl_2·2H_2O has been determined at −169 °C; crystallographic data and selected structural parameters are given in Tables 1−3, and a labeled figure and stereoview are provided in Figure 1. Treatment of complex **1** with 1 equiv of $(PhCO_2)_2$ in MeCN followed by addition of $NaClO_4$ leads to subsequent isolation of $[Mn_9Na_2O_7(O_2CPh)_{15}(MeCN)_2]$ (**3**) in acceptable yield (~31%). The single-crystal X-ray structure of **3**·MeCN has been determined at −170 °C; crystallographic data and selected structural parameters are given in Tables 1, 4, and 5, and a labeled figure and stereoview are provided in Figure 2. The $[Mn_8O_6]$ and $[Mn_9O_7]$ cores of complexes **2** and **3**, respectively, are compared in Figure 3.

Electrochemical studies on complexes **2** and **3** in CH_2Cl_2 solution have been performed using cyclic voltammetry (CV)

(21) *Theory and Applications of Molecular Paramagnetism*; Boudreaux, E. A., Mulay, L. N., Eds.; J. Wiley & Sons: New York, 1976.

(22) Schmitt, E. A.; Hendrickson, D. N. Unpublished results.

Table 3. Bond Angles (deg) for $(NBu^n_4)[Mn_8O_6Cl_6(O_2CPh)_7(H_2O)_2]$ (**2**)[a]

Cl(15)–Mn(1)–O(9)	85.74(25)	Cl(15)–Mn(7)–Cl(18)	171.45(13)
Cl(15)–Mn(1)–O(10)	86.01(24)	Cl(15)–Mn(7)–O(10)	83.45(23)
O(9)–Mn(1)–O(10)	84.0(3)	Cl(15)–Mn(7)–O(14)	84.34(22)
O(9)–Mn(2)–O(10)	82.2(3)	Cl(18)–Mn(7)–O(10)	95.21(23)
O(9)–Mn(2)–O(11)	96.9(3)	Cl(18)–Mn(7)–O(14)	87.21(23)
O(9)–Mn(2)–O(12)	175.3(3)	O(10)–Mn(7)–O(14)	89.7(3)
O(10)–Mn(2)–O(11)	174.5(3)	Cl(15)–Mn(8)–O(13)	86.62(25)
O(10)–Mn(2)–O(12)	97.5(3)	Cl(15)–Mn(8)–O(14)	86.28(25)
O(11)–Mn(2)–O(12)	83.0(3)	O(13)–Mn(8)–O(14)	88.3(3)
Cl(16)–Mn(3)–O(11)	85.39(24)	Mn(1)–Cl(15)–Mn(4)	70.03(9)
Cl(16)–Mn(3)–O(12)	86.23(25)	Mn(1)–Cl(15)–Mn(7)	69.99(9)
O(11)–Mn(3)–O(12)	84.2(3)	Mn(1)–Cl(15)–Mn(8)	110.15(11)
Cl(15)–Mn(4)–Cl(17)	170.30(12)	Mn(4)–Cl(15)–Mn(7)	106.86(10)
Cl(15)–Mn(4)–O(9)	83.13(23)	Mn(4)–Cl(15)–Mn(8)	69.91(9)
Cl(15)–Mn(4)–O(13)	84.49(24)	Mn(7)–Cl(15)–Mn(8)	70.29(9)
Cl(17)–Mn(4)–O(9)	96.82(24)	Mn(3)–Cl(16)–Mn(5)	72.57(10)
Cl(17)–Mn(4)–O(13)	85.81(24)	Mn(3)–Cl(16)–Mn(6)	72.59(10)
O(9)–Mn(4)–O(13)	89.5(3)	Mn(5)–Cl(16)–Mn(6)	105.00(13)
Cl(16)–Mn(5)–Cl(17)	173.63(13)	Mn(4)–Cl(17)–Mn(5)	78.09(10)
Cl(16)–Mn(5)–Cl(19)	91.00(13)	Mn(6)–Cl(18)–Mn(7)	77.29(10)
Cl(16)–Mn(5)–O(11)	82.76(23)	Mn(1)–O(9)–Mn(2)	96.6(3)
Cl(16)–Mn(5)–O(13)	95.16(23)	Mn(1)–O(9)–Mn(4)	113.1(4)
Cl(17)–Mn(5)–Cl(19)	94.71(13)	Mn(2)–O(9)–Mn(4)	115.1(4)
Cl(17)–Mn(5)–O(11)	91.54(24)	Mn(1)–O(10)–Mn(2)	96.2(3)
Cl(17)–Mn(5)–O(13)	81.73(23)	Mn(1)–O(10)–Mn(7)	113.6(4)
Cl(19)–Mn(5)–O(11)	173.74(25)	Mn(2)–O(10)–MN(7)	113.3(4)
Cl(19)–Mn(5)–O(13)	93.11(26)	Mn(2)–O(11)–Mn(3)	94.7(3)
O(11)–Mn(5)–O(13)	87.9(3)	Mn(2)–O(11)–Mn(5)	116.7(4)
Cl(16)–Mn(6)–Cl(18)	172.95(12)	Mn(3)–O(11)–Mn(5)	113.9(4)
Cl(6)–Mn(6)–Cl(20)	90.75(14)	Mn(2)–O(12)–Mn(3)	94.9(3)
Cl(16)–Mn(6)–O(12)	83.96(25)	Mn(2)–O(12)–Mn(6)	115.3(4)
Cl(16)–Mn(6)–O(14)	94.71(25)	Mn(3)–O(12)–Mn(6)	112.3(4)
Cl(18)–Mn(6)–Cl(20)	95.73(14)	Mn(4)–O(13)–Mn(5)	112.8(4)
Cl(18)–Mn(6)–O(12)	89.57(26)	Mn(4)–O(13)–Mn(8)	113.7(4)
Cl(18)–Mn(6)–O(14)	82.21(25)	Mn(5)–O(13)–Mn(8)	132.6(4)
Cl(20)–Mn(6)–O(12)	174.70(28)	Mn(6)–O(14)–Mn(7)	112.3(4)
Cl(20)–Mn(6)–O(14)	92.83(23)	Mn(6)–O(14)–Mn(8)	133.1(4)
O(12)–Mn(6)–O(14)	87.6(3)	Mn(7)–O(14)–Mn(8)	113.2(4)

[a] For the $[Mn_8O_6Cl_6]$ core only; a full listing is available in the supplementary material.

and differential pulse voltammetry (DPV). Only complex **2** displays reversible processes; both one-electron oxidation and reduction processes are observed at 0.91 and 0.12 V, respectively, *vs* ferrocene. The CV and DPV scans are shown in Figure 4.

The dc magnetic susceptibility measurements were made for a polycrystalline sample of complex **2** in a 10.0 kG field. When the temperature is decreased, $\chi_M T$ increases to a maximum value at 15.0 K and then decreases below 15.0 K (Figure 5). The effective magnetic moment per molecule (μ_{eff}) increases from 13.76 μ_B at 300.0 K to a maximum of 20.62 μ_B at 15.0 K and then decreases to 17.73 μ_B at 5.01 K. Complex **2** dc susceptibility data were also obtained in the 2.0–30.0 K range at magnetic fields of 5.00, 10.0, 20.0, 30.0, 40.0, and 50.0 kG. In Figure 6 is given a plot of reduced magnetization $M/N\mu_B$ (N is Avogadro's number, and μ_B is the Bohr magneton) *versus* the ratio of magnetic field H and absolute temperature T. At 50.0 kG and 2.0 K, the value of $M/N\mu_B$ was found to be 20.88. This magnetization saturation value is somewhat less than the $M/N\mu_B$ saturation value of 22 expected for a complex with a $S = 11$ ground state which has $g = 2.00$ and experiences no axial zero-field splitting ($D\hat{S}_z^2$).

The ac magnetic susceptibility measurements were made for a 124.7 mg polycrystalline sample of complex **2** in zero external field with a 1.0 G ac magnetic field oscillating at 500 Hz. In Figure 7 is given a plot of $\chi'_M T$ *versus* temperature, where χ'_M is the in-phase (real) component of the ac susceptibility. A maximum value of $\chi'_M T = 61.3(2)$ cm^3 K mol^{-1} occurs in the 3.6–6.4 K region. In contrast to the dc susceptibility data (Figure 5) there is no appreciable decrease in $\chi_M T$ at low temperatures. This is due to the fact that the ac data were collected in zero external field, whereas the dc data were collected at 10.0 kG. In the latter case the Zeeman interaction is significant and causes the decrease in $\chi_M T$ at low temperatures.

The dc magnetic susceptibility behavior of a polycrystalline sample of complex **3** is summarized in Figures 5 and 8. When the temperature is decreased, complex **3** in a 10.0 kG exhibits a gradually decreasing value of $\chi_M T$ (Figure 5). The effective magnetic moment per molecule decreases gradually from 12.23 μ_B at 320.0 K to 6.94 μ_B at 5.01 K. A plot of $M/N\mu_B$ *vs* H/T is shown in Figure 8 for complex **3** in the 2.0–4.0 K range in magnetic fields of 0.50, 1.00, 2.00, 3.00, 5.00, 10.0, and 20.0 kG. Reduced magnetization *vs* H/T data were also collected at 30.0, 40.0, and 50.0 kG in the 2.0–4.0 kG region.

Discussion

Compound Preparation. The preparation and structure of $(NBu^n_4)[Mn_4O_2(H_2O)(O_2CPh)_9]$ (**1**) have been described elsewhere.[19] This complex possesses a $[Mn_4O_2]^{8+}$ core with a bent or "butterfly" disposition of the four Mn^{III} ions. As such, it is a member of a family of such complexes that we have been describing over the last several years.[23] It differs, however, in having peripheral ligation consisting of *only* carboxylate (and water) ligation, *i.e.*, it has no O- and/or N-based chelates as found for previously described butterfly $[Mn_4O_2]^{8+}$ species which contain 2,2-bipyridine (bpy), 2-picolinate (pic), 8-hydroxyquinolinate (hqn), or deprotonated dibenzoylmethane (dbm). The latter have proven on several occasions to be excellent stepping-stones to other species with the same or higher nuclearities. Thus, $[Mn_4O_2(OAc)_6(py)_2(dbm)_2]$ reacts in MeCN with Cl^- to give distorted cubane $[Mn_4O_3Cl(OAc)_3(dbm)_3]$,[23b] whereas the same reaction in CH_2Cl_2 leads to $[Mn_7O_4(OAc)_{10}(dbm)_4]^-$ salts.[24] An analogous reaction with Br^- in MeCN yields $[Mn_4O_3Br(OAc)_3(dbm)_3]$.[25] Of particular relevance to the present work are reactions with Me_3SiCl; this carboxylate-abstraction reagent has been shown to often trigger subsequent disproportionation and/or nuclearity changes. Thus, treatment of $[Mn_4O_2(O_2CR)_7(pic)_2]^-$ in MeCN with Me_3SiCl leads to formation of $[Mn_8O_4(OAc)_{12}(pic)_4]$ if R is Me or $[Mn_4O_2(O_2CPh)_6(MeCN)_2(pic)_2]$ if R is Ph.[26a] In addition, treatment of $[Mn_4O_2(OAc)_7(bpy)_2]^+$ with Me_3SiCl leads to both disproportionation *and* a nuclearity change to give the remarkable complex $[Mn_{11}O_{10}Cl_2(OAc)_{11}(bpy)_2(H_2O)_2(MeCN)_2]^+$.[26b]

It is clear from the above brief summary that the reactions of $[Mn_4O_2]$ species with Me_3SiCl have proven to be a rich source of new products. It was logical, therefore, to examine what the analogous reaction with complex **1** might yield. Thus, Me_3SiCl was added to a solution of complex **1** in MeCN. No reaction appeared to occur, but subsequent isolation of the product established that a dramatic transformation and indeed taken place. The product was $(NBu^n_4)[Mn_8O_6Cl_6(O_2CPh)_7(H_2O)_2]$ (**2**), formed by an undoubtedly complicated mechanism involving destabilization *via* carboxylate abstraction, followed by fragmentation and reaggregation. Note, however, that no oxidation level change has resulted; both complexes **2** and **1**

(23) (a) Vincent, J. B.; Christmas, C.; Chang, H.-R.; Li, Q.; Boyd, P. D. W.; Huffman, J. C.; Hendrickson, D. N.; Christou, G. *J. Am. Chem. Soc.* **1989**, *111*, 2086. (b) Wang, S.; Folting, K.; Streib, W. E.; Schmitt, E. A.; McCusker, J. K.; Hendrickson, D. N.; Christou, G. *Angew. Chem., Int. Ed. Engl.* **1991**, *30*, 304. (c) Libby, E.; McCusker, J. K.; Schmitt, E. A.; Folting, K.; Hendrickson, D. N.; Christou, G. *Inorg. Chem.* **1991**, *30*, 3486. (d) Bouwman, E.; Bolcar, M. A.; Libby, E.; Huffman, J. C.; Folting, K.; Christou, G. *Inorg. Chem.* **1992**, *31*, 5185.

(24) Wang, S.; Tsai, H.-L.; Streib, W. E.; Christou, G.; Hendrickson, D. N. *J. Chem. Soc., Chem. Commun.* **1992**, 667.

(25) Wang, S.; Tsai, H.-L.; Streib, W. E.; Christou, G.; Hendrickson, D. N. *J. Chem. Soc., Chem. Commun.* **1992**, 1427.

(26) (a) Libby, E.; Folting, K.; Huffman, C. J.; Huffman, J. C.; Christou, G. *Inorg. Chem.* **1993**, *32*, 2549. (b) Perlepes, S. P.; Huffman, J. C.; Christou, G. *J. Chem. Soc., Chem. Commun.* **1991**, *23*, 1657.

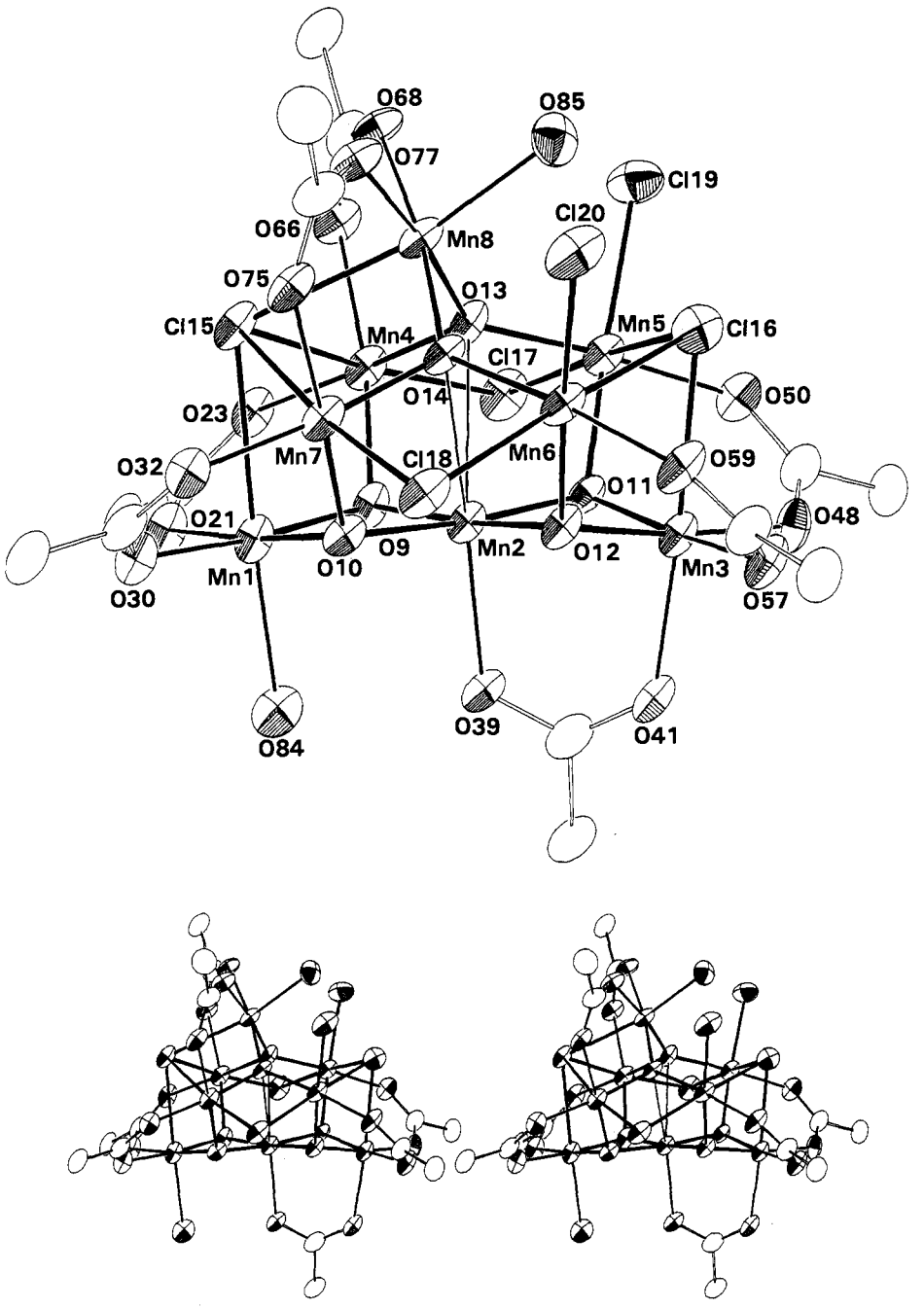

Figure 1. ORTEP representation and stereopair of the anion of complex **2** at the 50% probability level. For clarity, atoms not bound to Mn are de-emphasized.

contain only Mn^{III} ions (*vide infra*). An investigation of the dependence of the yield of complex **2** on the **1**:Me_3SiCl ratio indicated an optimal yield at a 1:4 ratio; a decrease in yield by approximately a factor of two resulted when ratios of 1:3 or 1:5 were employed. The overall transformation can be summarized by eq 1.

$$2[Mn_4O_2(H_2O)(O_2CPh)_9]^- + 8Me_3SiCl + 2H_2O \rightarrow [Mn_8O_6Cl_6(O_2CPh)_7(H_2O)_2]^- + 8Me_3SiO_2CPh + 3PhCO_2H + H^+ + 2Cl^- \quad (1)$$

In an attempt to direct a transformation of complex **1** to a Mn^{IV}-containing product, the reaction of this complex with dibenzoyl peroxide was explored. As in the transformation to give complex **2**, no reaction was immediately obvious, but addition of $NaClO_4$ was found to slowly give crystalline $[Mn_9Na_2O_7(O_2CPh)_{15}(MeCN)_2]$ in fair yield (~31%). There has again been no oxidation level change, the product containing nine Mn^{III} ions; the $(PhCO_2)_2$ is essential for the formation of complex **3**, however as shown by recovery of starting material on treatment of complex of **1** with $NaClO_4$ alone in MeCN. The function of $(PhCO_2)_2$ is unclear, although it does presumably trigger the transformation *via* an initial oxidation step. The low yield of complex **3** (~31%) suggests the formation of other Mn-containing reaction products, but we have found it difficult to isolate and identify other species in the mother liquor (filtrate).

Description of Structures. Complex **2**·3/2CH_2Cl_2·2H_2O crystallizes in the triclinic space group $P\bar{1}$ and contains discrete $[Mn_8O_6Cl_6(O_2CPh)_7(H_2O)_2]^-$ ions with no imposed symmetry. Selected bond distances and angles are listed in Tables 2 and 3; a complete listing is available in the supplementary material. The structure of the anion of complex **2** (Figure 1) consists of an $[Mn_8(\mu_3\text{-}O)_4(\mu_4\text{-}O)_2(\mu_2\text{-}Cl)_2(\mu_3\text{-}Cl)(\mu_4\text{-}Cl)]^{8+}$ core with peripheral ligation provided by bridging $PhCO_2^-$ and terminal Cl^- and H_2O groups. The $PhCO_2^-$ groups are all in their familiar

Table 4. Selected[a] Interatomic Distances (Å) for $Mn_9Na_2O_7(O_2CPh)_{15}(MeCN)_2$ (**3**)

Mn(1)−Mn(2)	2.886(2)	Mn(3)−O(12)	1.895(4)
Mn(1)−Mn(7)	3.318(2)	Mn(3)−O(143)	2.174(4)
Mn(1)−Mn(4)	3.359(2)	Mn(4)−O(10)	1.888(4)
Mn(2)−Mn(3)	2.871(2)	Mn(4)−O(16)	1.849(4)
Mn(2)−Mn(5)	3.241(2)	Mn(5)−O(11)	1.858(4)
Mn(2)−Mn(7)	3.261(2)	Mn(5)−O(16)	1.886(4)
Mn(2)−Mn(4)	3.311(2)	Mn(5)−O(64)	2.210(4)
Mn(2)−Mn(6)	3.318(2)	Mn(6)−O(12)	1.891(4)
Mn(2)−Mn(8)	3.388(2)	Mn(6)−O(15)	1.845(4)
Mn(2)−Mn(9)	3.393(2)	Mn(7)−O(13)	1.890(4)
Mn(3)−Mn(5)	3.315(2)	Mn(7)−O(15)	1.872(4)
Mn(3)−Mn(6)	3.358(2)	Mn(7)−O(37)	2.257(4)
Mn(4)−Mn(9)	3.324(2)	Mn(7)−O(100)	2.135(4)
Mn(4)−Mn(5)	3.369(2)	Mn(8)−O(14)	1.851(4)
Mn(5)−Mn(5)	2.999(2)	Mn(8)−O(15)	1.884(4)
Mn(6)−Mn(8)	3.248(2)	Mn(2)−O(37)	2.225(4)
Mn(6)−Mn(7)	3.382(2)	Mn(9)−O(14)	1.859(4)
Mn(7)−Mn(8)	3.007(2)	Mn(9)−O(16)	1.889(4)
Mn(8)−Mn(9)	3.281(2)	Mn(9)−O(64)	2.262(4)
Mn(1)−O(10)	1.893(4)	Na(152)−O(143)	2.407(4)
Mn(1)−O(13)	1.892(4)	Na(152)−O(12)	2.616(4)
Mn(1)−O(134)	2.180(4)	Na(152)−O(13)	2.598(4)
Mn(2)−O(10)	1.934(4)	Na(152)−O(100)	2.808(4)
Mn(2)−O(11)	1.906(4)	Na(153)−O(134)	2.390(4)
Mn(2)−O(12)	1.927(4)	Na(153)−O(10)	2.537(4)
Mn(2)−O(13)	1.911(4)	Na(153)−O(11)	2.824(4)
Mn(2)−O(14)	2.111(4)	Na(153)−O(73)	2.519(4)
Mn(3)−O(11)	1.884(4)		

[a] Core atoms only; excluding terminally-coordinated carboxylate oxygen and MeCN atoms.

Table 5. Bond Angles (deg) for $Mn_9Na_2O_7(O_2CPh)_{15}(MeCN)_2$ (**3**)

O(10)−Mn(1)−O(13)	82.43(16)	O(14)−Mn(8)−O(15)	88.69(16)
O(10)−Mn(1)−O(134)	86.26(15)	O(14)−Mn(8)−O(37)	91.36(15)
O(13)−Mn(1)−O(134)	90.99(15)	O(15)−Mn(8)−O(37)	84.70(16)
O(10)−Mn(2)−O(11)	92.56(15)	O(14)−Mn(9)−O(16)	88.00(16)
O(10)−Mn(2)−O(12)	155.69(15)	O(14)−Mn(9)−O(64)	90.04(16)
O(10)−Mn(2)−O(13)	80.86(15)	O(16)−Mn(9)−O(64)	84.38(15)
O(10)−Mn(2)−O(14)	105.46(15)	Mn(1)−O(10)−Mn(2)	97.95(16)
O(11)−Mn(2)−O(12)	81.32(15)	Mn(1)−O(10)−Mn(4)	125.31(20)
O(11)−Mn(2)−O(13)	146.87(16)	Mn(2)−O(10)−Mn(4)	120.04(19)
O(11)−Mn(2)−O(14)	104.29(15)	Mn(2)−O(11)−Mn(3)	98.49(17)
O(12)−Mn(2)−O(13)	91.43(16)	Mn(2)−O(11)−Mn(5)	118.83(20)
O(12)−Mn(2)−O(14)	98.85(15)	Mn(3)−O(11)−Mn(5)	124.76(20)
O(13)−Mn(2)−O(14)	108.77(15)	Mn(2)−O(12)−Mn(3)	97.37(16)
O(11)−Mn(3)−O(12)	82.76(16)	Mn(2)−O(12)−Mn(6)	120.68(19)
O(11)−Mn(3)−O(143)	88.85(15)	Mn(3)−O(12)−Mn(6)	124.95(20)
O(12)−Mn(3)−O(143)	85.79(16)	Mn(1)−O(13)−Mn(2)	98.76(17)
O(10)−Mn(4)−O(16)	86.26(17)	Mn(1)−O(13)−Mn(7)	122.67(20)
O(11)−Mn(5)−O(16)	89.57(17)	Mn(2)−O(13)−Mn(7)	118.14(19)
O(11)−Mn(5)−O(64)	92.70(16)	Mn(2)−O(14)−Mn(8)	117.39(19)
O(11)−Mn(5)−O(73)	87.17(15)	Mn(2)−O(14)−Mn(9)	117.33(18)
O(16)−Mn(5)−O(64)	85.92(15)	Mn(8)−O(14)−Mn(9)	124.42(20)
O(16)−Mn(5)−O(73)	87.47(15)	Mn(6)−O(15)−Mn(7)	130.94(22)
O(64)−Mn(5)−O(73)	173.40(15)	Mn(6)−O(15)−Mn(8)	121.14(20)
O(12)−Mn(6)−O(15)	87.52(16)	Mn(7)−O(15)−Mn(8)	106.38(19)
O(13)−Mn(7)−O(15)	91.12(16)	Mn(4)−O(16)−Mn(5)	128.84(21)
O(13)−Mn(7)−O(37)	89.65(15)	Mn(4)−O(16)−Mn(9)	125.55(21)
O(13)−Mn(7)−O(100)	91.36(16)	Mn(5)−O(16)−Mn(9)	105.19(18)
O(15)−Mn(7)−O(37)	84.08(15)	Mn(7)−O(37)−Mn(8)	84.27(14)
O(15)−Mn(7)−O(100)	92.26(16)	Mn(5)−O(64)−Mn(9)	84.21(14)
O(37)−Mn(7)−O(100)	176.21(15)		

syn,syn-bridging modes. The core can be conveniently described as containing a $[Mn_7O_4]$ subunit consisting of two $[Mn_4O_2]$ "butterfly" units [atoms Mn(1,2,4,7) and Mn(2,3,5,6)] fused by sharing a "hinge" or "body" Mn atom [Mn(2)]. The resultant $[Mn_3O_4]$ base is almost planar with Mn(1)−Mn(2)−Mn(3) = 172.5°. There are four bridging Cl atoms, Cl(15)−Cl(18), on the outside of the fused-butterfly unit; in addition, two oxygen atoms, O(13) and O(14), bridge the "wing-tip" Mn atoms, Mn(4)−Mn(7), on the inside and also connect to the eighth Mn atom, Mn(8) (Figures 1 and 3). This arrangement of the $[Mn_8O_6Cl_4]$ core would yield C_{2v} symmetry, with one mirror plane passing through Mn(2), O(13), O(14), and Mn(8), except that Mn(8) is tilted away from this plane and forms a bond to Cl(15). As a result, the peripheral ligation is also asymmetric, with two carboxylate groups bridging between Mn(8), Mn(4), and Mn(7), whereas the coordination sites on the other side are occupied by a terminal H_2O [O(85)] and by Cl atoms, Cl(19) and Cl(20). The symmetry of the whole anion consequently approximates to C_s, the mirror plane passing through Mn(1), Mn(2), Mn(3), and Mn(8). Note that the asymmetrically-disposed H_2O and $PhCO_2^-$ groups defined by O(84), O(39), and O(41) lie on the virtual mirror plane. All Mn atoms display Jahn−Teller (JT) axial distortion (elongation) as expected for high-spin Mn^{III} (d^4) in near-octahedral geometry. For Mn(4)−Mn(7), the JT axial sites are occupied by two *trans* Cl atoms; for Mn(8), atoms Cl(15) and O(85) are the axial ligands; and for Mn(1) and Mn(3), the JT sites are occupied by Cl(15), Cl(16), O(41), and O(84). The coordination about Mn(2) is discussed below.

There are two structural points that warrant further comment. Firstly, the coordination of Mn(8) to Cl(15) results in there being four different types of Cl-binding modes in the anion, *viz.*, terminal, μ, μ_3, and μ_4. More importantly, Cl (15) is an extremely rare example of a μ_4-Cl with tetragonal pyramidal geometry. As far as we have been able to determine, the only previous examples are in the anions $[V_5O_9(O_2CR)_4Cl]^{2-}$ [27a] and $[Hg_4Cl(C_2B_{10}H_{10})_4]^-$.[27b] In the anion of complex **2**, Cl (15) lies 1.602 Å above the Mn(1), Mn(4), Mn(7), and Mn(8) least-squares plane (deviation from which is 0.056 Å by all four Mn atoms). Quadruply-bridging Cl^- ions with *any* geometry are rather rare. In addition to the tetragonal pyramidal mode described above, examples are known of a μ_4-Cl bridging M_4 units with a tetrahedral[28] or butterfly[29] arrangement. A few higher denticity modes are also known.[30] Secondly, Mn(2) is better described as seven-coordinate, rather than five-coordinate, because there are clearly two weak bonds to O(13) and O(14). The resultant distances [Mn(2)−O(13), 2.676(7) Å; Mn(2)−O(14), 2.636(7) Å] are longer than the other Mn(2)−oxide bonds [1.900(7)−1.928(8) Å] but nevertheless represent significant interactions; note that if O(13) and O(14) are considered as occupying a single site, then O(39) and O(13)/O(14) are on the JT elongation axis. Mn(2)−O(39) [2.151(8) Å] is similar to the JT axially-elongated bond Mn(3)−O(41) [2.122(8) Å]. In addition, O(13) and O(14) may appear to be trigonal planar, but close inspection reveals that they lie 0.104 and 0.129 Å, respectively, out of their Mn_3 planes *toward* Mn(2), supporting weak interactions between them and the latter (see Figure 3). Thus, O(13) and O(14) are better described as possessing four-coordinate trigonal pyramidal geometry.

Complex **3**·3MeCN crystallizes in the triclinic space group $P\bar{1}$ and contains discrete $[Mn_9Na_2O_7(O_2CPh)_{15}(MeCN)_2]$ molecules with no imposed symmetry. Selected bond distances are listed in Tables 4 and 5; a complete listing is available in the supplementary material. The structure of complex **3** (Figure 2) displays several similarities to that of complex **2**. The

(27) (a) Heinrich, D. D.; Folting, K.; Streib, W. E.; Huffman, J. C.; Christou, G. *J. Chem. Soc., Chem. Commun.* **1989**, *28*, 4037. (b) Yang, X.; Knobler, C. B.; Hawthorne, M. F. *Angew. Chem., Int. Ed. Engl.* **1991**, *30*, 1507.

(28) (a) Dance, I. G. *J. Chem. Soc., Chem. Commun.* **1980**, 818. (b) Dance, I. G. *Aust. J. Chem.* **1985**, *38*, 1. (c) Trinh-Toan; Dahl, L. F. *Inorg. Chem.* **1976**, *15*, 2953.

(29) (a) Wuest, J. D.; Zacharie, B. *Organometallics* **1985**, *4*, 410. (b) Beauchamp, A. L.; Oliver, M. J.; Wuest, J. D.; Zacharie, B. *J. Am. Chem. Soc.* **1986**, *108*, 73.

(30) (a) Mikhalichko, B. M.; Olijnik, V. V.; Mys'kiv, M. G.; Zavalii, P. Yu. *Koord. Khim.* **1987**, *13*, 1536. (b) Schugar, H. J.; Ou, C.-C.; Thich, J. A.; Potenza, J. A.; Felthouse, T. R.; Haddad, M. S.; Hendrickson, D. N.; Furey, W.; Lalancette, R. A. *Inorg. Chem.* **1980**, *19*, 543. (c) Andersson, R. A.; Templeton, D. H.; Zalkin, A. *Inorg. Chem.* **1978**, *17*, 1961.

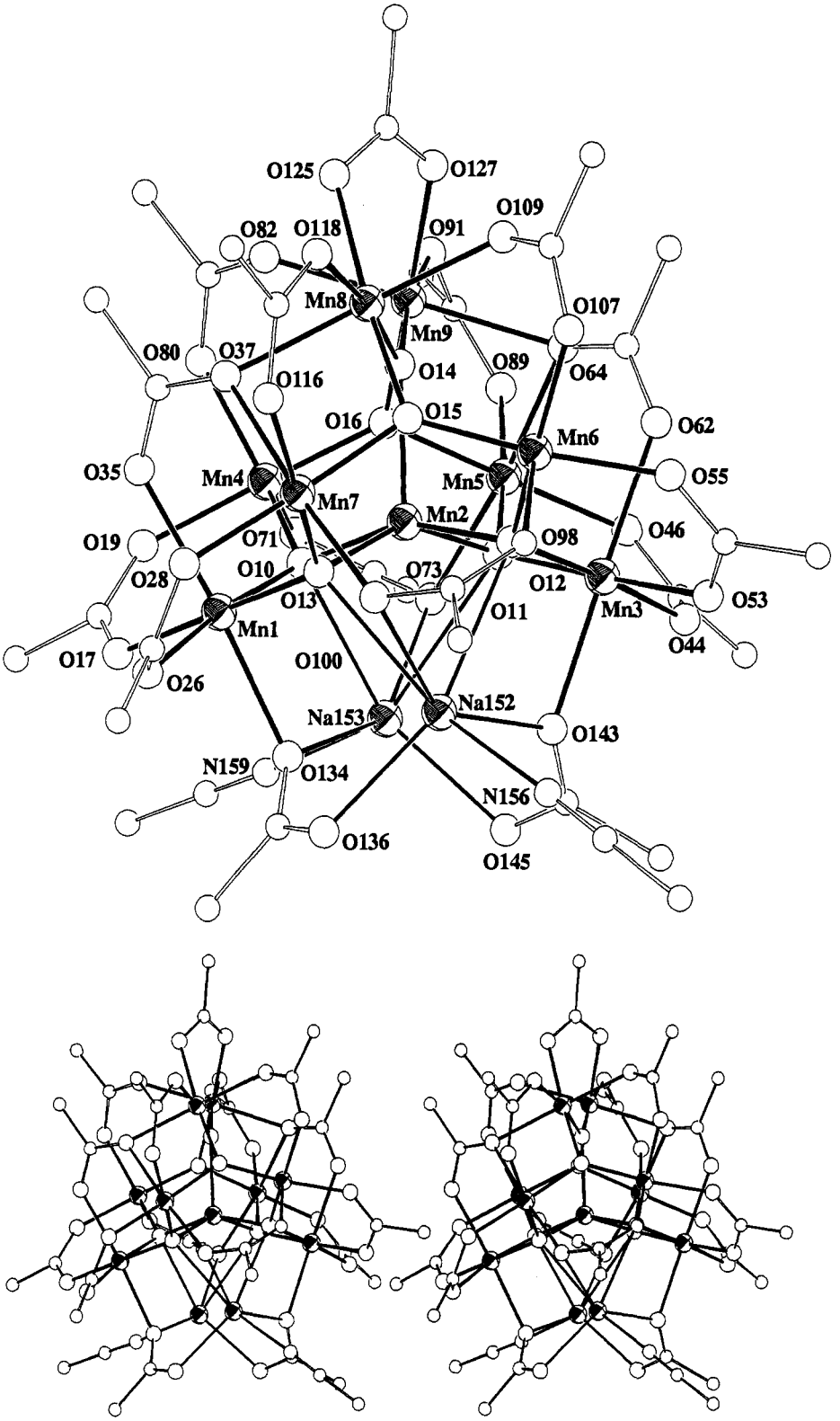

Figure 2. ORTEP representation and stereopair of complex **3** at the 50% probability level. For clarity, only metal atoms are emphasized.

$[Mn_9O_7]$ core can again be considered as containing a fused-butterfly unit formed by sharing of Mn atom Mn(2). Now, however, the $[Mn_3O_4]$ base is not planar but distinctly bent with Mn(1)−Mn(2)−Mn(3) = 140.5°. The remaining two Mn atoms, Mn(8) and Mn(9), are connected to the fused-butterfly unit by three μ_3-oxygen atoms O(14)−O(16). A comparison of the $[Mn_8O_6]$ and $[Mn_9O_7]$ cores of complexes **2** and **3**, respectively, provided in Figure 3 is from a viewpoint that emphasizes the means of connection of the extra Mn/O atoms to the $[Mn_7O_4]$ fused-butterfly base. Mn(2) is now truly five-coordinate and possesses square-pyramidal geometry. As for complex **2**, all octahedral Mn atoms display a clear JT axial elongation, with axial Mn−O bonds approximately 0.20 Å longer than equatorial Mn−O bonds. For Mn(2), the axial Mn-(2)−O(14) length [2.111(4) Å] is longer than basal lengths [1.906(4)−1.934(4) Å], as expected for SP geometry. Atoms Mn(4) and Mn(6) are also five-coordinate, but their coordination geometries are highly distorted from either the SP or TBP extremes.

Two Na atoms are connected to the $[Mn_9O_7]$ core *via* O atoms O(10)−O(13), and peripheral ligation to the $[Mn_9Na_2O_7]$ is provided by 15 $PhCO_2^-$ and two MeCN groups. Nine of the

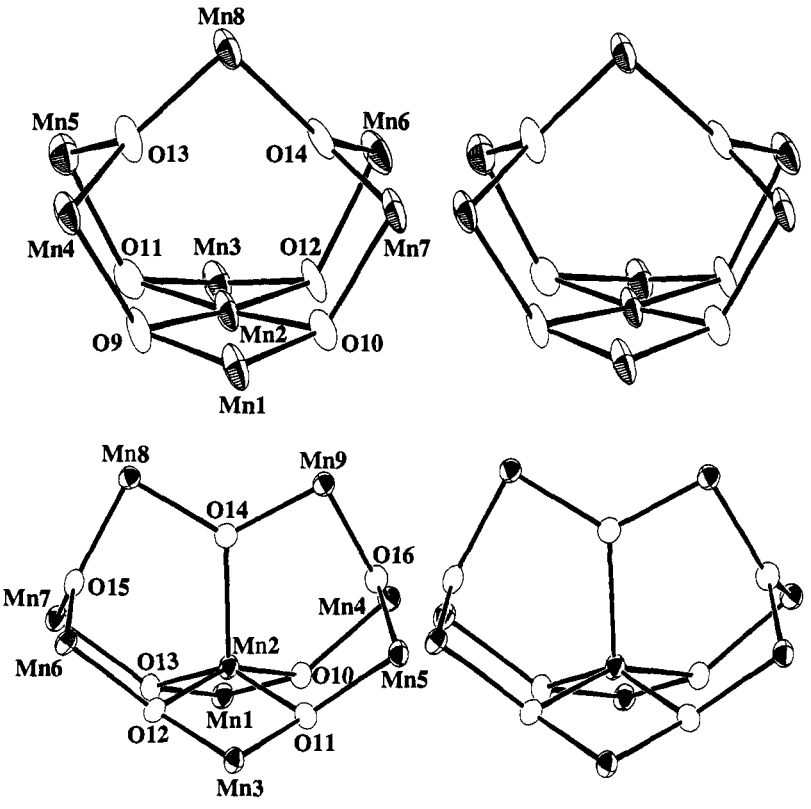

Figure 3. A comparison of the $[Mn_8O_6]$ and $[Mn_9O_7]$ cores of complexes **2** and **3**, respectively, from viewpoints approximately perpendicular to those in Figures 1 and 2.

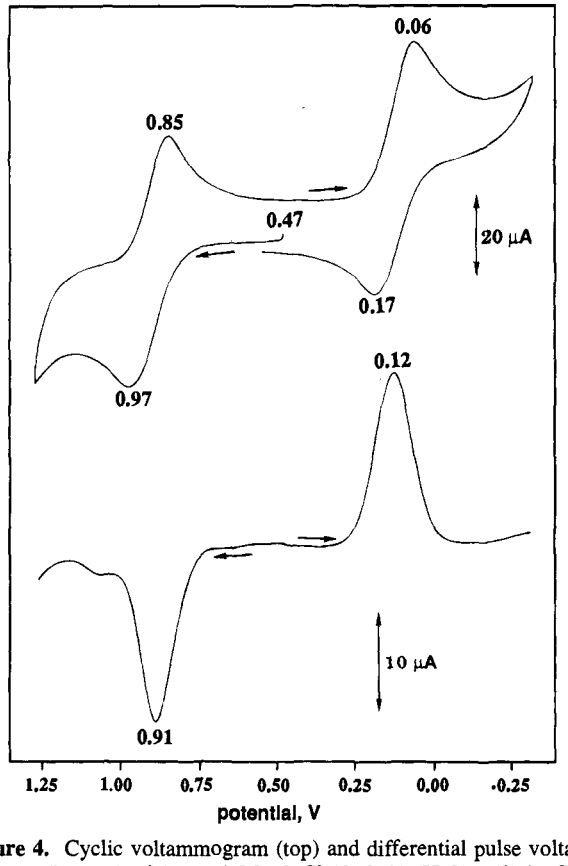

Figure 4. Cyclic voltammogram (top) and differential pulse voltammogram (bottom) of $(NBu^n_4)[Mn_8O_6Cl_6(O_2CPh)_7(H_2O)_2]$ (**2**) in CH_2Cl_2. The potentials are given *versus* the Cp_2Fe/Cp_2Fe^+ couple under the same conditions.

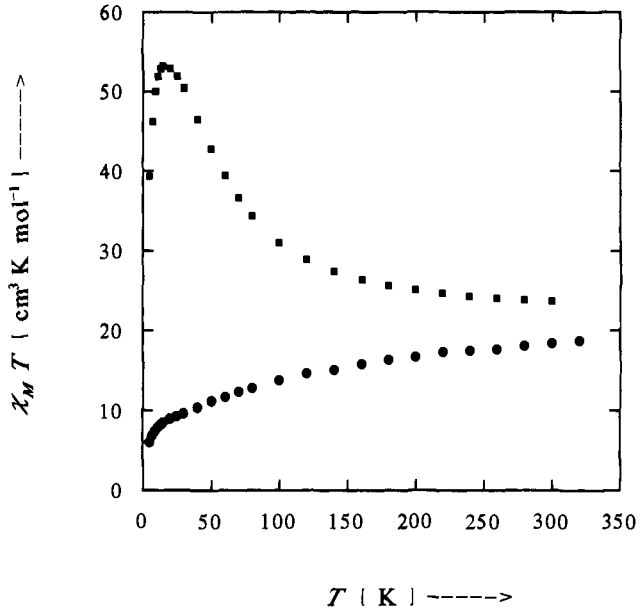

Figure 5. Plot of $\chi_M T$ versus temperature for polycrystalline samples of (■) $(NBu^n_4)[Mn_8O_6Cl_6(O_2CPh)_7(H_2O)_2]$ (**2**) and (●) $[Mn_9Na_2O_7(O_2CPh)_{15}(MeCN)_2]$ (**3**). χ_M is the molar dc magnetic susceptibility measured at 10.0 kG.

former are in the common *syn,syn*-μ-bridging mode, but the other six are in a rarer μ_3-bridging mode with one O atom bridging two metals. The two MeCN groups complete the distorted octahedral coordination at each Na atom. The complete molecule has virtual C_2 symmetry.

Owing to the close association between the Na atoms and the $[Mn_9O_7]$ core, the preferred description of complex **3** is as a molecular heterometallic undecanuclear aggregate rather than as an ion pair. Also known, however, is $[Mn_9O_7(O_2CPh)_{13}(py)_2]$, which is structurally identical to complex **3** except that the bottom $[Na_2(O_2CPh)_2(MeCN)_2]$ portion is replaced by terminal py groups on Mn(1) and Mn(3).[31]

(31) Low, D. W.; Eichhorn, D. M.; Draganescu, A.; Armstrong, W. H. *Inorg. Chem.* **1991**, *30*, 877.

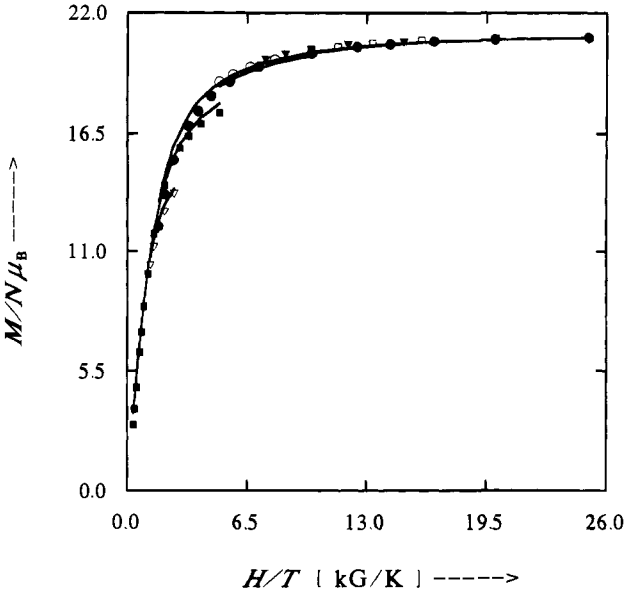

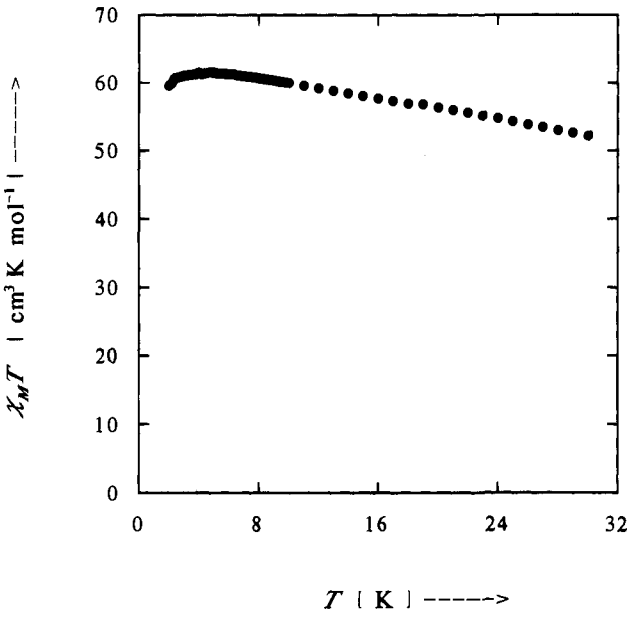

Electrochemial Studies. Complexes **2** and **3** have been investigated by cyclic voltammetry (CV) and differential pulse voltammetry (DPV). Complex **2** in CH_2Cl_2 solution displays two reversible processes, a one-electron oxidation at 0.91 V and a one-electron reduction at 0.12 V *vs* ferrocene. The CV and DPV responses are shown in Figure 4. The isolated complex is thus the central member of the electron transfer series in eq 2. With one exception,[32] mixed-valence II/III or III/IV

$$[\quad]^{0} \overset{0.91\ \text{V}}{\rightleftharpoons} [Mn_8O_6Cl_6(O_2CPh)_7(H_2O)]^{-} \overset{0.12\ \text{V}}{\rightleftharpoons} [\quad]^{2-} \quad (2)$$

$7Mn^{III}, Mn^{IV}$ $\qquad$ $8Mn^{III}$ $\qquad$ $Mn^{II}, 7Mn^{III}$

Mn_x aggregates are trapped-valence, probably owing to the increase in the barrier to intramolecular electron transfer resulting from the JT distortion of Mn^{III}. It is thus likely that the reduction and oxidation of complex **2** will be centered at a particular Mn atom, possibly Mn(2) for the oxidation since it is ligated to the greatest number of hard oxide ligands.

It is relatively rare for high-nuclearity $Mn/O/RCO_2^-$ aggregates to exhibit reversible redox processes, the $[Mn_{12}O_{12}(O_2CR)_{16}(H_2O)_4]$ complexes being the only previous examples.[13] In fact, the redox behaviors of complex **2** and $[Mn_{12}O_{12}(O_2CPh)_{16}(H_2O)_4]$ (**4**) are very similar; the latter in CH_2Cl_2 has reversible one-electron oxidation and reduction waves at 0.79

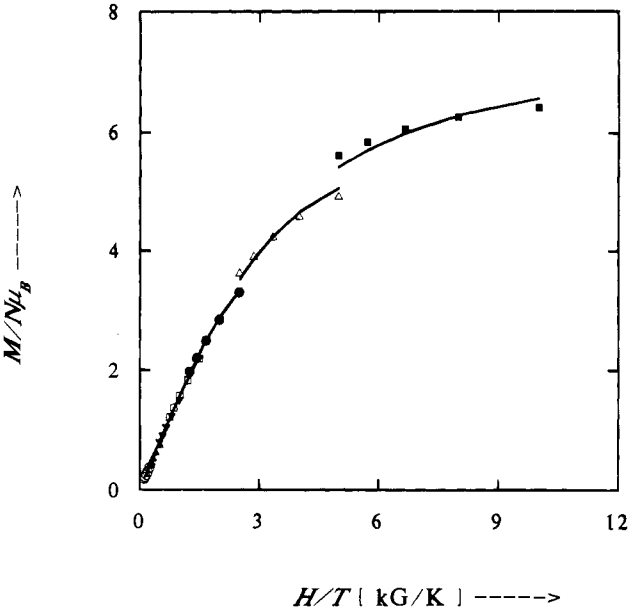

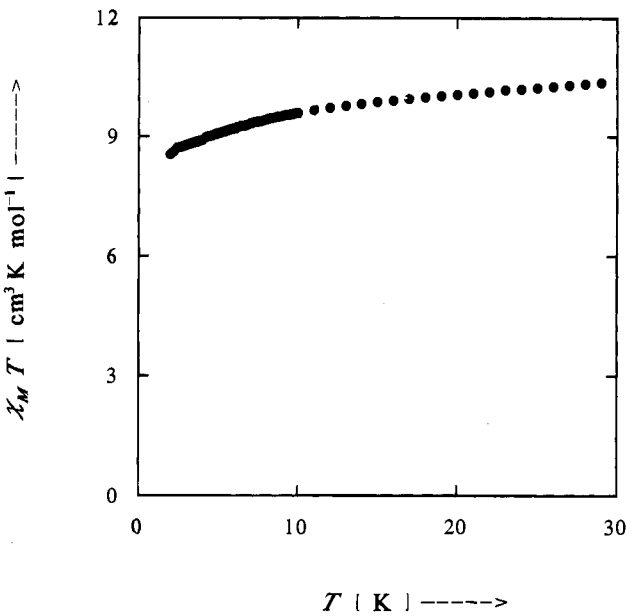

(32) (a) Jang, H. G.; Vincent, J. B.; Nakano, M.; Huffman, J. C.; Christou, G.; Sorai, M.; Wittebort, R. J.; Hendrickson, D. N. *J. Am. Chem. Soc.* **1989**, *111*, 7778. (b) Nakano, M.; Sorai, M.; Vincent, J. B.; Christou, G.; Jang, H. G.; Hendrickson, D. N. *Inorg. Chem.* **1989**, *28*, 4608.

and 0.11 V, respectively, values quite similar to those of complex **2**. Reduction of complex **4** with $NR_4^+I^-$ (R = various) or PPh_4I has allowed isolation of the monoanion in a pure, highly-crystalline form; also, the $EtCO_2^-$ version has recently been structurally characterized.[33] Attempts are currently in progress to generate and crystallize the reduced version of complex **2** in an analogous manner.

In contrast to the reversible behavior by complex **2**, complex **3** shows only broad, irreversible features in the CV and DPV scans, two oxidations at ~0.51 and 0.88 V and multiple reductions in the range of −0.2 to −0.8. This behavior is more typical of Mn carboxylate aggregates.

Magnetochemistry of Complex 2. The effective magnetic moment for this Mn^{III}_8 complex is 13.76 μ_B at 300.0 K, which is close to the spin-only value (g = 2.0) of 13.86 μ_B expected for a Mn^{III}_8 complex that does not exhibit intramolecular magnetic exchange interactions. When the temperature of complex **2** is decreased (Figure 5), μ_{eff} increases to 20.62 μ_B at 15.0 K. This stands in marked contrast to the behavior of $Mn^{III}_4O_2$ butterfly complexes, where, for example, for the butterfly complex $(NBu^n_4)[Mn_4O_2(O_2CMe)_7(pic)_2]$, μ_{eff} per molecule gradually decreases from 7.98 μ_B at 300.0 K to 6.35 μ_B at 25.0 K.[23c] The increase in μ_{eff} with decreasing temperature for complex **2** in a 10.0 kG field is very reminiscent of the behavior of $[Mn_{12}O_{12}(O_2CR)_{16}(H_2O)_4]$ [R = Ph (**4**), R = Me (**5**), and R = Et (**6**)].[13,33] These three $Mn^{IV}_4Mn^{III}_8$ complexes show a maximum (19−20 μ_B) in μ_{eff}/molecule *vs* temperature at 10−20 K. This was attributed to the population of a large-spin ground state at the lowest temperatures. Complex **5** was shown to have a S = 10 ground state, while complexes **4** and **6** have S = 9 ground states.

Confirmation that complex **2** does indeed have a large-spin ground state was obtained by means of the low-temperature, variable-field magnetization data depicted in Figure 6. Data were collected for complex **2** in the 2.0−30.0 K range and at fields of 5.00, 10.0, 20.0, 30.0, 40.0, and 50.0 kG. In Figure 6 it can be seen that these six isofield data sets nearly superimpose on a plot of $M/N\mu_B$ *vs* H/T. If there were only one state populated in the 2.0−30.0 K range and if this state had g = 2.0 and experienced no zero-field splitting, then the $M/N\mu_B$ *vs* H/T plot would follow a Brillouin function that would asymptotically approach a value of $2S$, where S is the spin of the ground state. From Figure 6 it can be seen that for complex **2** at 2.0 K and 50.0 kG the value of $M/N\mu_B$ is 20.88. Since complex **2** only has integer spin states, this suggested that complex **2** has a S = 11 ground state.

The reduced magnetization data for complex **2** (Figure 6) were least-squares fitted to quantitatively characterize the ground state of this complex. In order to least-squares fit these data, it was assumed that a ground state of spin S is the only state populated in the 2.0−4.0 K range, and the magnetization for the complex was then calculated with eq 3:

$$M = N\sum_{i=1}^{P}\left(\frac{-\delta E_i}{\delta H}\right)\exp(-E_i/kT)/\sum_{i=1}^{P}\exp(-E_i/kT) \qquad (3)$$

In this equation N is Avogadro's number, and $\delta E_i/\delta H$ is the change in energy of the ith level in response to a change in the magnetic field. The energies of the various sublevels ($\pm M_S$) of the ground state are obtained by diagonalization of the spin Hamiltonian matrix on each iteration which includes the Zeeman and axial zero-field ($D\hat{S}_z^2$) interactions. The solid lines in Figure 6 represent the least-squares fit of the six isofield magnetization data sets for complex **2**. The best fit was found with S = 11, D = −0.040 cm^{-1}, and g = 1.92. If the data are fitted with the spin of the ground state being taken as either S = 12 or S = 10, then very unreasonable values (g < 1.5 and g > 2.6, respectively) for the g parameter result. The Mn^{III}_8 complex **2** has a S = 11 ground state.

The zero-field splitting parameter D for the ground state of complex **2** is relatively small. Qualitative evidence for this comes from the near superimposition of the six isofield magnetization data sets (Figure 6). The $[Mn_{12}O_{12}(O_2CR)_{16}(H_2O)_4]$ complexes exhibit S = 9 or S = 10 ground states that have a larger zero-field splitting. For example, the R = CH_3 complex (5) has a S = 10 ground state with $D \simeq -0.5$ cm^{-1}.[14b]

The zero-field splitting in the ground state of a polynuclear Mn^{III}_x complex is largely a projection of the single-ion zero-field interactions present for the Mn^{III} ions in the complex. Each Mn^{III} ion generally experiences a Jahn−Teller distortion, where two ligand atoms are found at longer bond distances than the other four ligand atoms. The two ligand atoms with the longer bond lengths lie on the z-axis for each Mn^{III} ion. This same z-axis is usually the principal axis for the paramagnetic structure (*i.e.*, g-tensor, susceptibility tensor, and D-tensor). The magnitude of the single-ion zero-field interaction (D parameter) reflects crystal-field effects and spin−orbital admixture of excited states occurring for each Mn^{III} ion. Thus, in a polynuclear Mn^{III}_x complex, the magnetic exchange interactions that are present couple all the spins of the Mn^{III} ions together in a certain fashion to give a ground state of a given spin. The vectorial projection of the zero-field interactions at each Mn^{III} ion in the complex dictates the value of D for the ground state. In other words, if all the Jahn−Teller axes of the Mn^{III} ions in the complex are parallel, then the ground state will likely have a relatively large zero-field splitting. If there is a misalignment (perpendicular) of the Jahn−Teller axes of the various Mn^{III} ions, then a relatively small zero-field splitting will result.

In the case of the $[Mn_{12}O_{12}(O_2CR)_{16}(H_2O)_4]$ complexes, the eight Mn^{III} ions are arranged in a ring about the central $Mn^{IV}_4O_4$ cubane unit.[13,33] The Jahn−Teller axes of the eight Mn^{III} ions are nearly parallel for all of these Mn_{12} complexes, and this explains the relatively large zero-field splitting in the S = 9 or S = 10 ground states. Reference to Figure 1, however, shows that the Jahn−Teller axes of the Mn^{III} ions in complex **2** are not all aligned. Those of Mn(1), Mn(2), and Mn(3) are near to parallel, but the axes of the "wing-tip" ions Mn(4), Mn(5), Mn(6), and Mn(7) are disposed in a nearly perpendicular fashion. The net result is that the S = 11 ground state of complex **2** experiences a relatively small zero-field splitting.

The ac magnetic susceptibility data for complex **2** were obtained for two reasons. First, susceptibility measurements can be carried out in zero external field with an ac susceptometer. It was important to check if complex **2** has a S = 11 ground state in zero external field. Second, ac susceptibility can be used to probe relaxation effects. In the ac susceptibility experiment the direction of the magnetic field is varied at a known frequency. The small amplitude (1×10^{-3} G) of the ac field allows an accurate determination of the magnetic microstructure, while the possibility of varying the frequency of the oscillating field adds important information about the dynamics in the magnetic system. The three $[Mn_{12}O_{12}(O_2CR)_{16}(H_2O)_4]$ complexes and $(PPh_4)[Mn_{12}O_{12}(O_2CEt)_{16}(H_2O)_4]$ are the only molecular complexes reported to show an out-of-phase ac susceptibility signal.[13,14,33] The last complex resulted from a one-electron reduction of complex **6** and has a valence-trapped $Mn^{IV}_4Mn^{III}_7Mn^{II}$ structure with a $S = {}^{19}/_2$ ground state.[33] Two features of these four complexes give rise to the out-of-phase ac signal. Not only do they have large-spin ground states, but these ground states also have relatively large zero-field splittings

(33) Eppley, H. J.; Tsai, H.-L.; de Vries, N.; Folting, K.; Christou, G.; Hendrickson, D. N. *J. Am. Chem. Soc.* **1995**, *117*, 301.

as discussed above. Thus, when the ac field is moved from being parallel to being perpendicular to the magnetic z-axis of these complexes, there is an appreciable difference in the interaction (Zeeman plus zero-field). If the ac field is moved at some frequency and there is little thermal energy (*i.e.*, low temperatures), then the magnetization of each Mn_{12} complex cannot stay in phase with the oscillating field. There is thus an in-phase as well as an out-of-phase ac magnetic susceptibility signal.

In Figure 7 is given a plot of $\chi'_M T$ *versus* temperature for complex **2**, where χ'_M is the in-phase component of the ac susceptibility. These data were collected in zero external dc magnetic field and with a 1.0 G ac field oscillating at 500 Hz. At low temperatures, there is a plateau in $\chi'_M T$ at a value of 61.3(2) cm^3 K mol^{-1}. This is consistent with a $S = 11$ ground state with $g = 1.93$. Even though the measurements were carried out down to 2.0 K, there is no evidence of the onset of relaxation effects in the $\chi'_M T$ *versus* temperature data for the complex. For the above four Mn_{12} complexes which exhibit relaxation effects, plots of their $\chi'_M T$ *versus* temperature responses exhibit a relatively abrupt decrease in $\chi'_M T$ below a certain temperature.[13,14,33] As can be seen in Figure 7, the data for complex **2** are quite different, and complex **2** does *not* show an out-of-phase ac magnetic susceptibility in the 2.0−30.0 K range. It is likely that the relatively small zero-field splitting in the $S = 11$ ground state is the reason for the absence of an out-of-phase ac susceptibility signal for complex **2**.

Magnetochemistry of Complex 3. Even though there are similarities in the molecular structures of complexes **2** and **3**, Figure 5 shows that there is an appreciable difference in their magnetic susceptibility characteristics. $\chi_M T$ for $[Mn_9Na_2O_7(O_2CPh)_{15}(MeCN)_2]$ (**3**) in a 10.0 kG field decreases with decreasing temperature. It is clear that the spin of the ground state for Mn^{III}_9 complex **3** is considerably less than that for complex **2**.

From an analysis of the reduced magnetization ($M/N\mu_B$) *versus* H/T data for complex **3** (Figure 8) we have concluded that the ground state of complex **3** has $S = 4$. The reduced magnetization data for complex **3** taken at 2.0−4.0 K in fields of 0.50, 1.00, 2.00, 3.00, 5.00, 10.0, and 20.0 kG were least-squares fitted to give a $S = 4$ ground state with $g = 1.94$ and $D = -0.25$ cm^{-1}. The solid lines in Figure 8 show that this fit is good. Reduced magnetization data were also collected for complex **3** at 30.0, 40.0, and 50.0 kG in the 2.0−4.0 K range. When these data (available in supplementary material) are included together with the 0.50−20.0 kG data, the least-squares fit is *not* as good. It appears that there are low-lying excited states. In the larger fields of 30.0−50.0 kG these excited states affect the $M/N\mu_B$ data.

The ac magnetic susceptibility data for complex **3** in zero external dc field in the 2.0−30.0 K range (Figure 9) are also consistent with a $S = 4$ ground state. A $S = 4$ state with $g = 2.00$ would be expected to give a $\chi'_M T$ value of 10.00 cm^3 K mol^{-1}. As with complex **2** these ac data were obtained in a 1.0 G ac field oscillating at 500 Hz. Finally, we found that complex **3** also does *not* exhibit an out-of-phase ac signal, again consistent with low magnetic anisotropy resulting from the nonparallel alignment of the nine Jahn−Teller axes within the molecule.

Origin of Differences in Ground States of Complexes 2 and 3. As described above, there are similarities in the molecular structures of complexes **2** and **3**, yet the spins of the ground states are quite different. In this section we will give a qualitative rationalization of why the ground-state spins differ so much.

As indicated above (Figure 3), complexes **2** and **3** can each be described as containing $[Mn_7O_4]^{13+}$ subunits consisting of two $[Mn_4O_2]^{8+}$ "butterfly" units fused by sharing a "body" Mn atom. The magnetic exchange characteristics of three different $[Mn_4O_2]^{8+}$ "butterfly" complexes have been described.[23,34] The core of the "butterfly" complex is as follows:

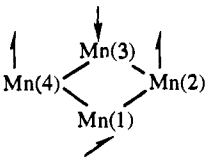

There are two different exchange parameters: a body−body interaction parameter J_{13} and a wing-tip−body parameter $J_{12} = J_{23} = J_{14} = J_{34} \equiv J$. By least-squares fitting the variable-temperature dc magnetic susceptibility data for three complexes it has been found that both types of interaction are antiferromagnetic and that $|J_{13}|$ is appreciably larger than $|J|$. All three Mn^{III}_4 "butterfly" complexes have a ground state with $S = 3$. Even though both types of pairwise exchange interactions are antiferromagnetic, the ground state of these complexes has six unpaired electrons. This results from spin frustration. Because the body−body J_{13} interaction is greater than the wing-tip−body interaction J, the spins on the Mn(1) and Mn(3) ions have a greater tendency to pair up. Each wing-tip Mn^{III} ion interacts with both the Mn(1) and Mn(3) ions and would align its spin antiparallel to both if possible, but it cannot do so. The net result is that the spin alignments of the wing-tip ions are frustrated. Overall, the unpaired electrons on the Mn(1) and Mn(3) atoms are essentially paired up (actually the resultant spin vector $\mathbf{S}_{13} = 1$ as shown above, not $\mathbf{S}_{13} = 0$), and this leaves the unpaired electrons on the wing-tip ions.

It is interesting that, in the case of the known $[Fe_4O_2]^{8+}$ "butterfly" complexes,[35] the spin frustration is different. In this case, $|J| > |J_{13}|$, and this gives a different spin alignment:

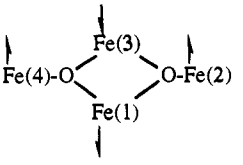

Thus, the domination of the wing-tip−body interaction leads to a $S = 0$ ground state for the Fe^{III}_4 "butterfly" complexes. This reversal in spin frustration from the Mn^{III}_4 to the Fe^{III}_4 "butterfly" complexes may provide some insight about why complex **2** has a $S = 11$ ground state, whereas complex **3** has a $S = 4$ ground state.

The $[Mn_7O_4]^{13+}$ subunit of complex **2** may have the following approximate spin orientations:

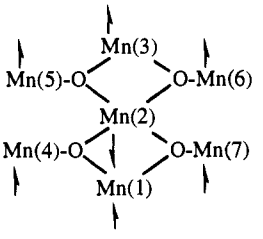

In complex **2**, the Mn(1), Mn(2), and Mn(3) atoms are in the same plane as the four O atoms in the unit. This should lead to a spin frustration that is the same as that for the three known $Mn^{III}_4O_2$ butterflies. Thus, the spins on the two body atoms

(34) Hendrickson, D. N. In *Research Frontiers in Magnetochemistry*; O'Connor, C. J., Ed.; World Scientific Publishing Co.: Singapore, 1993.
(35) McCusker, J. K.; Vincent, J. B.; Schmitt, E. A.; Mino, M. L.; Shin, K.; Coggin, D. K.; Hagen, P. M.; Huffman, J. C.; Christou, G.; Hendrickson, D. N. *J. Am. Chem. Soc.* **1991**, *113*, 3012.

should in each "butterfly" unit have the greater tendency to pair up, and this would give a net spin of $S(\text{body}) = 2$ for the fused body atoms Mn(1), Mn(2), and Mn(3) in the $[Mn_7O_4]^{13+}$ subunit. The spins on the four wing-tip atoms are frustrated, and thus each would have a spin of 2. This gives $S(\text{wing-tip}) = 8$ if they are all aligned. Coupling of $S(\text{body})$ and $S(\text{wing-tip})$ in this scheme would give $S = 10$, which then could couple with the last Mn^{III} ion [Mn(8)] to give a total spin of $S = 8-12$. It is, of course, not possible to predict the magnitudes of all of the exchange interactions present in the anion of complex **2**, and the above discussion merely suggests how the spin frustration known to be present in a $Mn^{III}_4O_2$ "butterfly" complex might lead to the $S = 11$ ground state observed for the anion of complex **2**.

In complex **3** the central $[Mn_3O_4]$ base of the $[Mn_3O_4]$ base of the $[Mn_7O_4]^{13+}$ subunit is distinctly bent (Figure 3) and the Mn(2) atom is five-coordinate with a square-pyramidal geometry. In complex **2** this Mn(2) atom is effectively six-coordinate. The distortions at Mn(2) in complex **3** would likely weaken the body–body interactions and possibly make it such that the spin frustration in each "butterfly" subunit could be more like that in a $Fe^{III}_4O_2$ "butterfly". That is, for complex **3** the wing-tip–body type interaction (J) could be stronger than the body–body interaction. This could lead to a different spin frustration, schematically pictured as follows:

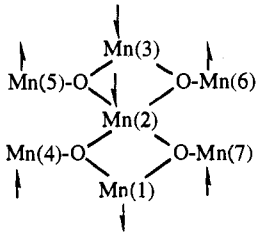

In this case the vectorial sum of the body spins would give $S(\text{body}) = 6$ and the sum of the wing-tip spins $S(\text{wing-tip}) = 8$. If these vectorial resultants couple antiferromagnetically, this would give $S = 2$ for the $[Mn_7O_4]^{13+}$ subunit. In complex **3**, the Mn(8) and Mn(9) atoms also have $S = 2$ each suggesting a total S of 2–6. This discussion is only intended to qualitatively show a possible origin of the $S = 4$ ground state observed for complex **3**. It is clear that calculations employing the full spin Hamiltonian are required in order to fit the susceptibility data and to explain in detail why these two complexes have ground states with such different spin values. This is, however, a major task that would require considerable effort and time.

Acknowledgment. This work was supported by NSF Grants CHE-9115286 (D.N.H.), CHE-9420322 (D.N.H.), and CHE-9311904 (G.C.) and by NIH Grant GM-39083 (G.C.). The ac magnetic susceptibility measurements were performed with an ac SQUID susceptometer in the Center for Interface and Material Science (University of California–San Diego), which was funded by the W. A. Keck Foundation.

Supplementary Material Available: Tables of magnetic susceptibility and magnetization data and complete listings of bond lengths and angles and thermal positional parameters for complexes **2** and **3** (63 pages); listing of observed and calculated structure factors (59 pages). This material is contained in many libraries on microfiche, immediately follows this article in the microfilm version of the journal, can be ordered from the ACS, and can be downloaded from the Internet; see any current masthead page for ordering information and Internet access instructions.

JA942828P